Submitted to the
XXII International Symposium on Lepton-Photon Interactions at High Energy
30 June - 5 July, Uppsala, Sweden

Abstract: 254 **Session: EW&B**

Measurement of high-Q^2 deep inelastic scattering cross sections with longitudinally polarised positron beams at HERA

ZEUS Collaboration

Abstract

The first measurements of the cross sections for neutral and charged current deep inelastic scattering in e^+p collisions with longitudinally polarised positron beams are presented. The total cross section for e^+p charged current deep inelastic scattering is presented at positive and negative values of positron beam longitudinal polarisation. In addition, single differential cross sections are presented for charged and neutral current deep inelastic scattering in the kinematic region $Q^2 > 200\,\mathrm{GeV}^2$. The measurements are based on data of integrated luminosity $30.5\,\mathrm{pb}^{-1}$ collected with the ZEUS detector in 2003 and 2004 at a centre-of-mass energy of 318 GeV. The measured cross sections are compared with the predictions of the Standard Model.

1 Introduction

Deep inelastic scattering (DIS) of leptons off nucleons has proved to be a key tool in the understanding of the structure of the proton and the form of the Standard Model (SM). The HERA ep collider has made possible the exploration of DIS at high values of four-momentum-transfer squared, Q^2. Using data taken in the years 1994-2000 the H1 and ZEUS collaborations have reported measurements of the cross sections for charged current (CC) and neutral current (NC) DIS [1–18]. These measurements extend the kinematic region covered by fixed-target experiments [19–22] to higher Q^2 and allow the HERA experiments to probe the electroweak sector of the Standard Model.

This paper presents the first measurements of the cross sections for e^+p CC and NC DIS with longitudinally polarised positron beams. The measurements are based on $16.4\,\mathrm{pb}^{-1}$ of data collected at a mean luminosity weighted polarisation of -40.2%, and $14.1\,\mathrm{pb}^{-1}$ collected at a polarisation of 31.8% with the ZEUS detector in 2003 and 2004. During this time HERA collided protons of energy 920 GeV with positrons of energy 27.5 GeV, yielding collisions at a centre-of-mass energy of 318 GeV. The measured cross sections are compared to the Standard Model predictions.

2 Kinematic variables and cross sections

Inclusive deep inelastic lepton-proton scattering can be described in terms of the kinematic variables x, y and Q^2. The variable Q^2 is defined to be $Q^2 = -q^2 = -(k - k')^2$ where k and k' are the four-momenta of the incoming and scattered lepton, respectively. Bjorken x is defined by $x = Q^2/2P \cdot q$ where P is the four-momentum of the incoming proton. The variable y is defined by $Q^2 = sxy$, where $s = 4E_eE_p$ is the square of the lepton-proton centre-of-mass energy (neglecting the masses of the incoming particles).

The electroweak Born level cross section for the CC reaction, $e^+p \to \bar{\nu}_e X$, with a longitudinally polarised positron beam (defined in Eqn. (1)), can be expressed as [23]

$$\frac{d^2\sigma^{CC}(e^+p)}{dxdQ^2} = (1+\mathcal{P})\frac{G_F^2}{4\pi x}\left(\frac{M_W^2}{M_W^2+Q^2}\right)^2 \cdot \left[Y_+F_2^{CC}(x,Q^2) - Y_-xF_3^{CC}(x,Q^2) - y^2F_L^{CC}(x,Q^2)\right],$$

where G_F is the Fermi constant, M_W is the mass of the W boson and $Y_\pm = 1 \pm (1-y)^2$. The structure functions F_2^{CC} and xF_3^{CC} contain sums and differences of the quark and anti-quark parton density functions (PDFs) and F_L^{CC} is the longitudinal structure function. The longitudinal polarisation of the positron beam is defined as

$$\mathcal{P} = \frac{N_R - N_L}{N_R + N_L}, \tag{1}$$

where N_R and N_L are the numbers of right and left-handed positrons in the beam. Similarly the cross section for the NC reaction, $e^+p \to e^+X$, can be expressed as

$$\frac{d^2\sigma^{NC}(e^+p)}{dxdQ^2} = \frac{2\pi\alpha^2}{xQ^4}[H_0^+ + \mathcal{P}H_{\mathcal{P}}^+],$$

where α is the QED coupling constant and H_0^+ and $H_{\mathcal{P}}^+$ contain the unpolarised and polarised structure functions, respectively.

Charged current events are characterised by a large missing transverse momentum, $P_{T,\text{miss}}$, which is calculated as

$$P_{T,\text{miss}}^2 = P_x^2 + P_y^2 = \left(\sum_i E_i \sin\theta_i \cos\phi_i\right)^2 + \left(\sum_i E_i \sin\theta_i \sin\phi_i\right)^2,$$

where the sum runs over all calorimeter energy deposits E_i, and θ_i and ϕ_i are the polar and azimuthal angles of the calorimeter cell as viewed from the interaction vertex. The hadronic polar angle, γ_h, is defined by $\cos\gamma_h = (P_{T,\text{miss}}^2 - \delta^2)/(P_{T,\text{miss}}^2 + \delta^2)$, where $\delta = \sum(E_i - E_i\cos\theta_i) = \sum(E - P_z)_i$. In the naive Quark Parton Model, γ_h gives the scattering angle of the struck quark in the lab frame. The total transverse energy, E_T, is given by $E_T = \sum E_i \sin\theta_i$.

Neutral current events are characterised by the presence of a high-energy isolated scattered positron in the detector. It follows from longitudinal momentum conservation that for well measured NC events δ peaks at twice the positron beam energy i.e. 55 GeV.

The kinematic variables for charged current events were reconstructed from the measured $P_{T,\text{miss}}$ and δ using the Jacquet-Blondel method [24]. The double-angle method [25] was used for the neutral current events to estimate the kinematic variables from the polar angles of the scattered positron and the hadronic final state.

In the following, measurements of total cross-sections and differential cross-sections in x, y and Q^2 for the charged current reaction are presented. In addition, differential cross-sections in Q^2 were measured for the neutral current reaction.

3 Monte Carlo simulation

Monte Carlo simulation (MC) was used to determine the efficiency for selecting events, the accuracy of kinematic reconstruction, to estimate the background rate and to deduce

cross sections for the full kinematic region from the data. A sufficient number of events were generated to ensure that uncertainties from MC statistics were small. The MC samples were normalised to the total integrated luminosity of the data.

Neutral and charged current DIS events including radiative effects were simulated using the DJANGOH [26] generator. The hadronic final state was simulated using the colour-dipole model of ARIADNE 4.10 [27] and, as a systematic check, the MEPS model of LEPTO 6.5 [28]. Both programs use the Lund string model of JETSET 7.4 [29] for the hadronisation. Photoproduction background was estimated using events simulated with HERWIG 5.9 [30]. Diffractive NC events were generated using the RAPGAP 2.08/06 [31] program and mixed with the non-diffractive MC events in order to simulate accurately the hadronic final state.

4 Event selection

4.1 Charged current

The following criteria were imposed to select charged current events and reject background.

- Missing transverse momentum: $P_{T,\mathrm{miss}} > 12\,\mathrm{GeV}$ was required and, in addition, the missing transverse momentum, excluding the calorimeter cells adjacent to the forward beam hole, $P'_{T,\mathrm{miss}}$, was required to exceed $10\,\mathrm{GeV}$;
- Primary vertex: events were required to satisfy $|Z_{\mathrm{VTX}}| < 50$ cm. The Z coordinate of the *ep* interaction vertex, reconstructed using tracks in the central tracking detector (CTD), was required to be in the centre of the detector. For events with an hadronic angle, γ_h, of less than 23° the vertex position was set to the nominal value of zero, and the $P_{T,\mathrm{miss}}$ and $P'_{T,\mathrm{miss}}$ thresholds increased to 14 and 12 GeV, respectively;
- Rejection of photoproduction: $P_{T,\mathrm{miss}}/E_T > 0.4$ was required for events with $20 < P_{T,\mathrm{miss}} < 30\,\mathrm{GeV}$; $P_{T,\mathrm{miss}}/E_T > 0.55$ was required for events with $P_{T,\mathrm{miss}} < 20\,\mathrm{GeV}$. These requirements demanded an azimuthally collimated energy flow. In addition, it was required that the angle between the missing transverse momentum measured by the CTD tracks and that measured by the calorimeter was less than one radian;
- Rejection of NC DIS: NC DIS events with a poorly measured scattered positron or hadronic jet can have significant missing transverse momentum. Events with $\delta > 30\,\mathrm{GeV}$ and an isolated electromagnetic cluster in the calorimeter were rejected;
- Rejection of non-*ep* background: interactions between the beams and residual gas in the beam pipe or upstream accelerator components can lead to events with signifi-

cant missing transverse momentum, however for these interactions the arrival times of energy deposits in the calorimeter are inconsistent with the bunch crossing time. The arrival times were used to reject such events. Muon finding algorithms based on tracking, calorimeter and muon chamber information were used to reject events caused by cosmic rays or muons in the beam halo. In addition, the shape of hadronic showers in the calorimeter was used to reject halo muon events depositing energy in the forward calorimeter;

- Kinematic region: events were required to satisfy $Q^2_{\rm JB} > 200\,{\rm GeV}^2$ and $y_{\rm JB} < 0.9$. These requirements restricted the event sample to a kinematic region where the resolution of the kinematic quantities is good and the background is small.

A total of 604 candidate events passed the selection criteria. The background contamination was estimated to be typically less than 1% but was as high as 5% in the lowest Q^2 bin of the negative polarisation sample. Figure 1 shows a comparison of data and MC distributions for the CC sample. The Monte Carlo gives a good description of the data.

4.2 Neutral current

The following criteria were imposed to select neutral current events.

- Positron identification: an algorithm which combined information from the energy deposits in the calorimeter with tracks measured in the CTD was used to identify scattered positrons. A fiducial-volume cut was applied to guarantee that the experimental acceptance was well understood. To ensure high purity and reject background, the identified positron was required to have an energy of at least 10 GeV and be isolated such that the energy in an $\eta - \phi$ cone of radius 0.8 centered on the positron, not associated with the positron, was less than 5 GeV. For events in which a positron was found within the acceptance of the CTD a track matched to the energy deposit in the calorimeter was required. For events with a positron at a smaller polar angle than the acceptance of the CTD the track requirement was replaced with the requirement that the transverse momentum of the positron exceeded 30 GeV;
- Primary vertex: events were required to satisfy $|Z_{\rm VTX}| < 50$ cm. The Z coordinate of the ep interaction vertex, reconstructed using tracks in the central tracking detector, was required to be in the centre of the detector;
- Background rejection: the requirement $38 < \delta < 65\,{\rm GeV}$ was imposed to remove photoproduction and beam-gas events, and to reduce the number of events with significant QED initial state radiation. The lower threshold was increased to 44 GeV for events which did not have a track matched to the positron candidate. To further reduce background from photoproduction events, y calculated from the electron method (y_e)

was required to satisfy $y_e < 0.95$. The net transverse momentum is expected to be small, so in order to remove cosmic-ray events and beam related background events the quantity $P_T/\sqrt{E_T}$ was required to be less than $4\sqrt{\text{GeV}}$, and the quantity P_T/E_T was required to be less than 0.7;

- QEDC rejection: to reduce the size of the QED radiative corrections, elastic Compton scattering events were rejected;
- Kinematic region: to avoid regions of phase space in which the MC generator is not valid the quantity $y_{\text{JB}}(1-x_{\text{DA}})$ was required to be greater than 0.004. In addition the final event sample was defined by requiring $Q^2_{\text{DA}} > 200\,\text{GeV}^2$.

A total of 52004 candidate events passed the selection criteria. The background contamination was estimated to be typically less than 1%. Figure 2 shows a comparison of data and MC expectation distributions for the NC sample. The Monte Carlo gives a generally good description of the data. Inaccuracies in the simulation of the scattered positron energy distribution are considered in the corresponding systematic uncertainty. The effects of the positron fiducial-volume cut can be seen in the distribution of the scattered positron angle.

5 Systematic uncertainties

The major sources of systematic uncertainty in the CC cross sections were the calorimeter energy scale and the uncertainty in the parton-shower scheme. The former was estimated by varying the energy scale of the whole calorimeter by the error in the energy scale, $\pm$ 2%. The resulting shifts in the cross sections were typically less than 10%, but increased to 20% in the highest Q^2 bin and 30% in the highest x bin. To estimate the sensitivity of the results to the details of the simulation of the hadronic final state, the LEPTO MEPS model was used instead of the ARIADNE model for calculating the acceptance corrections. The largest effects of $\sim 5\%$ were observed in the highest Q^2 and x bins. The systematic effects of the selection cuts were estimated by varying the threshold value of each selection cut independently by around 10%, which is a reasonable match to the resolution. The resulting shifts in the cross sections were typically within $\pm 5\%$.

The major source of systematic uncertainty in the NC cross section was the uncertainty in the parton-shower scheme which gave changes in the cross section of typically 2-3% but up to 10% at high Q^2. Uncertainty in the electromagnetic energy scale was estimated by varying the energy scale by $\pm(2-3)\%$, however, due to the use of the double-angle reconstruction, the resulting shifts in the cross section were typically $< 0.5\%$. The systematic effects of the selection cuts were estimated by varying the threshold value of each selection

cut independently by typically 10%, which is a reasonable match to the resolution. The resulting shifts in the cross sections were typically within ±2%.

The individual uncertainties were added in quadrature separately for the positive and negative deviations from the nominal cross section values to obtain the total systematic uncertainty. The positron beam polarisation was measured using the HERA Compton polarimeters. The uncertainty in the measured polarisation was 1.6-5% using the longitudinal polarimeter and 3.5% using the transverse polarimeter. The uncertainty in the measured luminosity was 5%. The uncertainties in the luminosity and polarisation measurements were not included in the total systematic uncertainty.

6 Results

The total cross section for e^+p CC DIS in the kinematic region $Q^2 > 200\,\mathrm{GeV}^2$ was measured at longitudinal positron beam polarisations of $31.8 \pm 0.9\%$ and $-40.2 \pm 1.1\%$ to be

$$46.7 \pm 2.4(\mathrm{stat.}) \pm 1.0(\mathrm{syst.})\mathrm{pb},$$

and

$$22.5 \pm 1.6(\mathrm{stat.}) \pm 0.5(\mathrm{syst.})\mathrm{pb},$$

respectively. The total cross section is shown as a function of the longitudinal polarisation of the positron beam in Fig. 3 including the unpolarised ZEUS measurement from the 1999-2000 data [17]. The data are compared to the Standard Model prediction evaluated using the ZEUS-S PDFs [32]. The SM prediction describes the data well. The cross section points at polarisations of 31.8% and -40.2% respectively are 3.4 standard deviations above and 6.1 below the unpolarised measurement, respectively.

The single-differential cross-sections, $d\sigma/dQ^2$, $d\sigma/dx$ and $d\sigma/dy$ for charged current DIS are shown in Fig. 4. A clear difference is observed between the measurements for positive and negative longitudinal polarisation, which is well described by the Standard Model evaluated using the ZEUS-S PDFs.

Figure 5 shows the cross-section $d\sigma/dQ^2$ for NC DIS for positive and negative longitudinal polarisations. In Fig. 6 ratios of the cross sections for the positive and negative longitudinal polarisations to the unpolarised results [18] are shown. Also shown is the ratio of the cross sections for the positive and negative longitudinal polarisations. Only statistical uncertainties were considered when taking ratios of the positively and negatively

polarised cross sections. In taking ratios to the unpolarised cross sections the systematic uncertainties were considered uncorrelated with those of the polarised cross sections. The measurements are well described by the SM evaluated using the ZEUS-S PDFs and consistent with the expectations of the electroweak Standard Model for polarised NC DIS, although the statistical precision of the current data set does not allow the polarised effect to be conclusively observed.

7 Summary

The cross sections for neutral and charged current deep inelastic scattering in e^+p collisions with longitudinally polarised positron beams have been measured. The measurements are based on data of integrated luminosity $30.5\,\mathrm{pb}^{-1}$ collected with the ZEUS detector in 2003 and 2004 at a centre-of-mass energy of 318 GeV. The total cross section for e^+p charged current deep inelastic scattering is presented at positive and negative values of positron beam longitudinal polarisation. In addition, single differential cross sections are presented for charged and neutral current deep inelastic scattering in the kinematic region $Q^2 > 200\,\mathrm{GeV}^2$. The measured cross sections are well described by the predictions of the Standard Model.

Acknowledgements

It is a pleasure to thank H. Spiesberger and T. Abe for useful discussions.

References

[1] H1 Coll., T. Ahmed et al., Phys. Lett. **B 324**, 241 (1994).

[2] H1 Coll., S. Aid et al., Z. Phys. **C 67**, 565 (1995).

[3] H1 Coll., S. Aid et al., Phys. Lett. **B 379**, 319 (1996).

[4] H1 Coll., S. Aid et al., Nucl. Phys. **B 470**, 3 (1996).

[5] H1 Coll., C. Adloff et al., Nucl. Phys. **B 497**, 3 (1997).

[6] H1 Coll., C. Adloff et al., Eur. Phys. J. **C 13**, 609 (2000).

[7] H1 Coll., C. Adloff et al., Eur. Phys. J. **C 19**, 269 (2001).

[8] H1 Coll., C. Adloff et al., Eur. Phys. J. **C 21**, 33 (2001).

[9] H1 Coll., C. Adloff et al., Eur. Phys. J. **C 30**, 1 (2003).

[10] ZEUS Coll., M. Derrick et al., Phys. Rev. Lett. **75**, 1006 (1995).

[11] ZEUS Coll., M. Derrick et al., Z. Phys. **C 72**, 47 (1996).

[12] ZEUS Coll., J. Breitweg et al., Eur. Phys. J. **C 11**, 427 (1999).

[13] ZEUS Coll., J. Breitweg et al., Eur. Phys. J. **C 12**, 411 (2000). Erratum in Eur. Phys. J. **C 27**, 305 (2003).

[14] ZEUS Coll., S. Chekanov et al., Eur. Phys. J. **C 21**, 443 (2001).

[15] ZEUS Coll., S. Chekanov et al., Phys. Lett. **B 539**, 197 (2002). Erratum in Phys. Lett. **B 552**, 308 (2003).

[16] ZEUS Coll., S. Chekanov et al., Eur. Phys. J. **C 28**, 175 (2003).

[17] ZEUS Coll., S. Chekanov et al., Eur. Phys. J. **C 32**, 1 (2003).

[18] ZEUS Coll., S. Chekanov et al., Phys. Rev. **D 70**, 052001 (2004).

[19] CDHS Coll., H. Abramowicz et al., Z. Phys. **C 25**, 29 (1984).

[20] CDHSW Coll., J.P. Berge et al., Z. Phys. **C 49**, 187 (1991).

[21] CCFR Coll., E. Oltman et al., Z. Phys. **C 53**, 51 (1992).

[22] BEBC Coll., G.T. Jones et al., Z. Phys. **C 62**, 575 (1994).

[23] R.J. Cashmore et al., *Proc. the Workshop on Future Physics at HERA*, G. Ingelman, A. De Roeck and R. Klanner (eds.), Vol. 1, p. 163. DESY, Hamburg, Germany (1996).

[24] F. Jacquet and A. Blondel, *Proceedings of the Study for an ep Facility for Europe*, U. Amaldi (ed.), p. 391. Hamburg, Germany (1979). Also in preprint DESY 79/48.

[25] S. Bentvelsen, J. Engelen and P. Kooijman, *Proc. Workshop on Physics at HERA*, W. Buchmüller and G. Ingelman (eds.), Vol. 1, p. 23. Hamburg, Germany, DESY (1992);
K.C. Höger, *Proc. Workshop on Physics at HERA*, W. Buchmüller and G. Ingelman (eds.), Vol. 1, p. 43. Hamburg, Germany, DESY (1992).

[26] G.A. Schuler and H. Spiesberger, *Proc. Workshop on Physics at HERA*, W. Buchmüller and G. Ingelman (eds.), Vol. 3, p. 1419. Hamburg, Germany, DESY (1991);
H. Spiesberger, HERACLES *and* DJANGOH*: Event Generation for ep Interactions at HERA Including Radiative Processes*, 1998, available on `http://www.desy.de/~hspiesb/djangoh.html`.

[27] L. Lönnblad, Comp. Phys. Comm. **71**, 15 (1992).

[28] G. Ingelman, A. Edin and J. Rathsman, Comp. Phys. Comm. **101**, 108 (1997).

[29] T. Sjöstrand, Comp. Phys. Comm. **39**, 347 (1986);
T. Sjöstrand and M. Bengtsson, Comp. Phys. Comm. **43**, 367 (1987);
T. Sjöstrand, Comp. Phys. Comm. **82**, 74 (1994).

[30] G. Marchesini et al., Comp. Phys. Comm. **67**, 465 (1992).

[31] H. Jung, Comp. Phys. Comm. **86**, 147 (1995).

[32] ZEUS Coll., S. Chekanov et al., Phys. Rev. **D 67**, 012007 (2003).

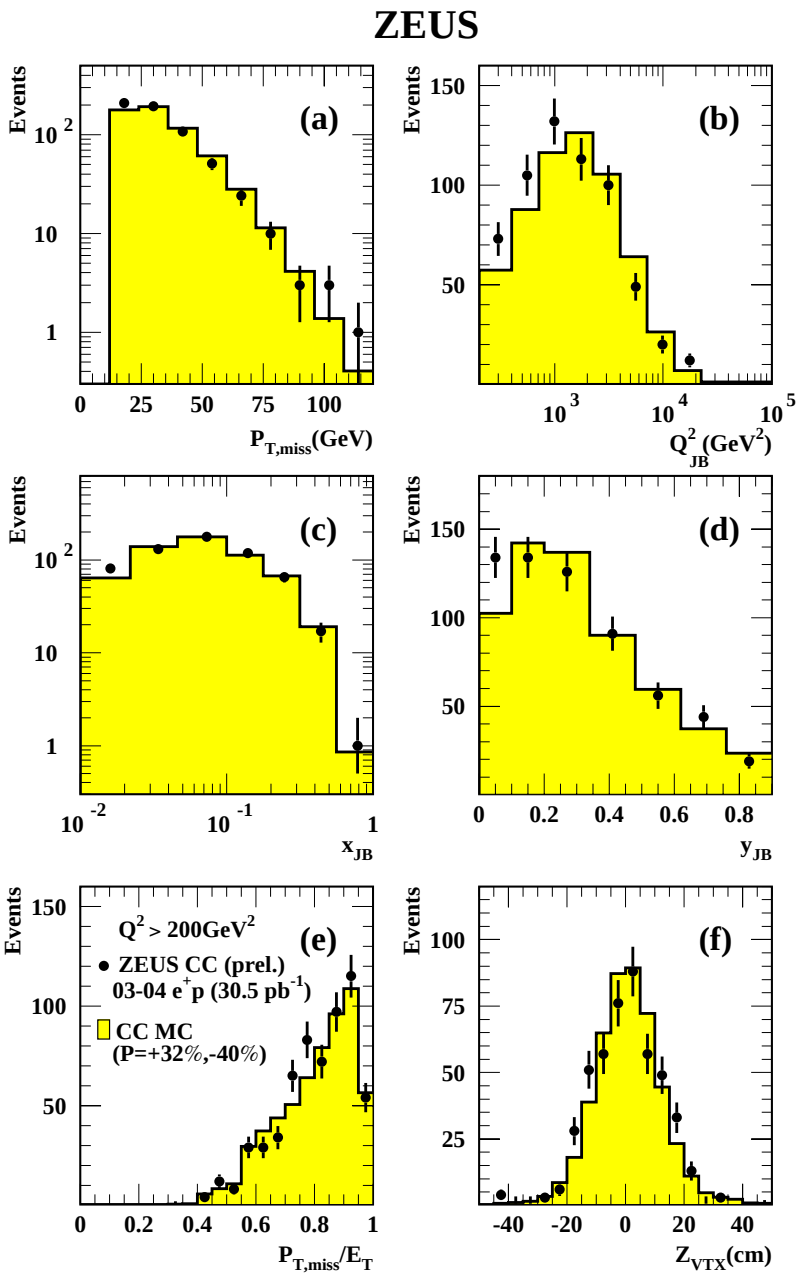

Figure 1: *Comparison of the final e^+p CC data sample with the expectations of the Monte Carlo simulation described in the text. The distributions of (a) missing transverse momentum, $P_{T,\mathrm{miss}}$, (b) Q^2_{JB}, (c) x_{JB}, (d) y_{JB}, (e) $P_{T,\mathrm{miss}}/E_T$ and (f) the Z coordinate of the event vertex, Z_{VTX}, are shown.*

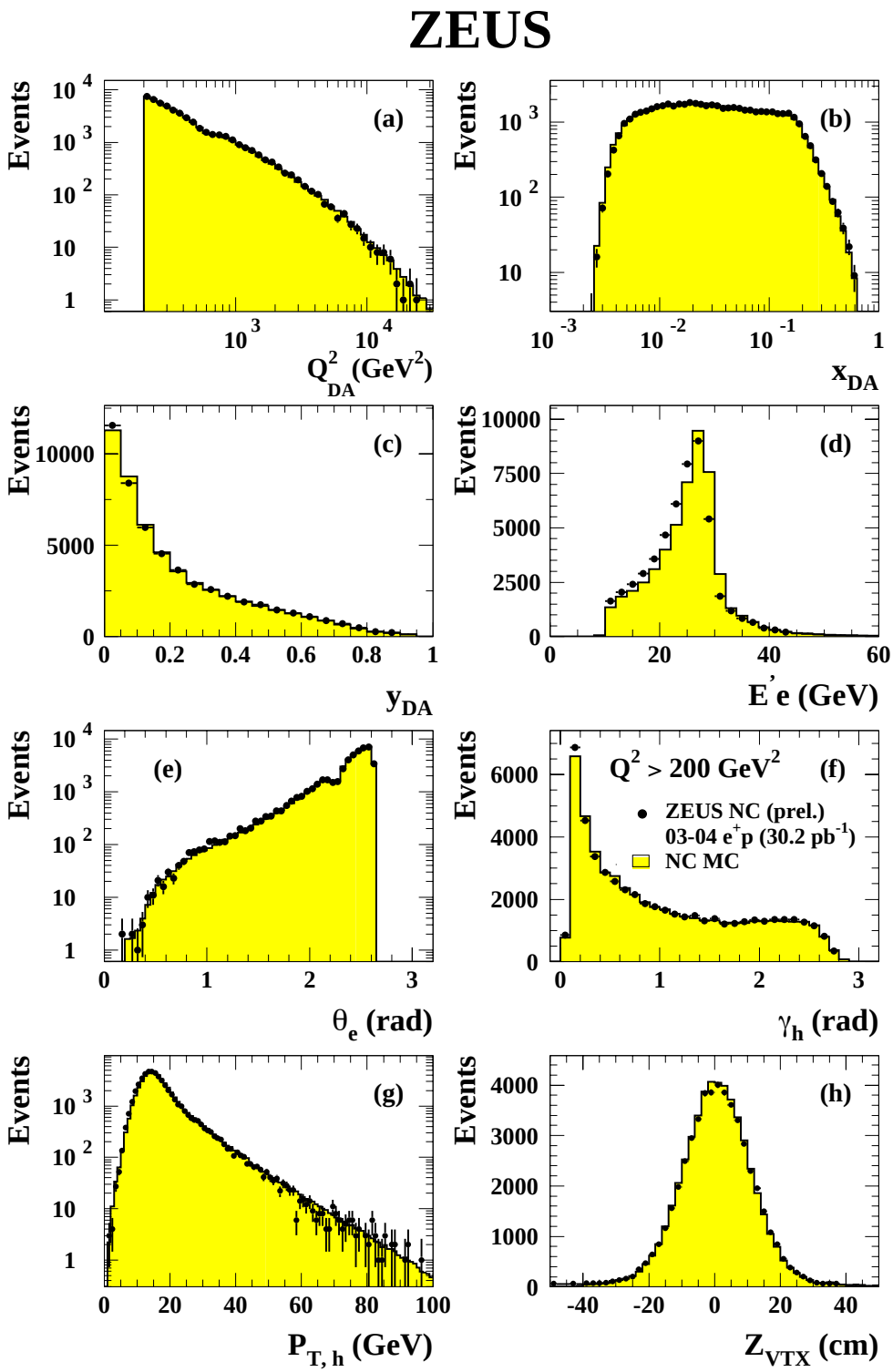

Figure 2: *Comparison of the final e^+p NC data sample with the expectations of the Monte Carlo simulation described in the text. The distributions of (a) $Q^2_{\rm DA}$, (b) $x_{\rm DA}$, (c) $y_{\rm DA}$, (d) the energy of the scattered positron, E'_e, (e) the angle of the scattered positron, θ_e, (f) the hadronic angle , γ_h, (g) the transverse momentum of the hadronic system, $P_{T,h}$, and (h) the Z coordinate of the event vertex, Z_{VTX}, are shown.*

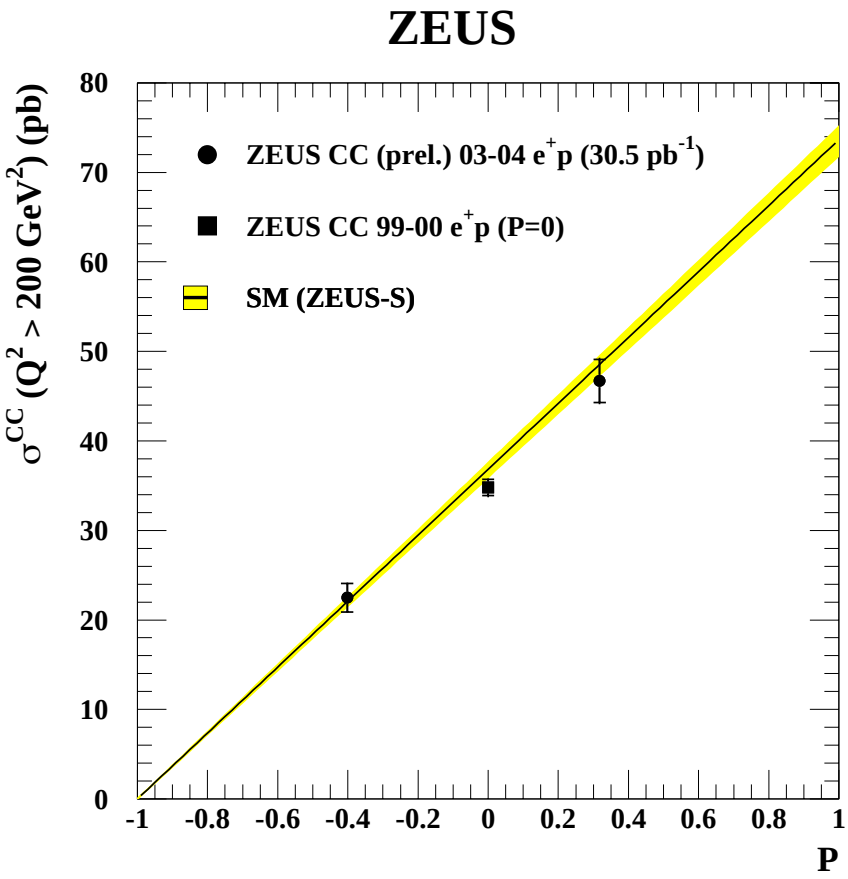

Figure 3: *The total cross section for e^+p CC DIS as a function of the longitudinal polarisation of the positron beam. The line shows the prediction of the SM evaluated using the ZEUS-S PDFs and the shaded band indicates the uncertainty on the cross section from the ZEUS-S fit.*

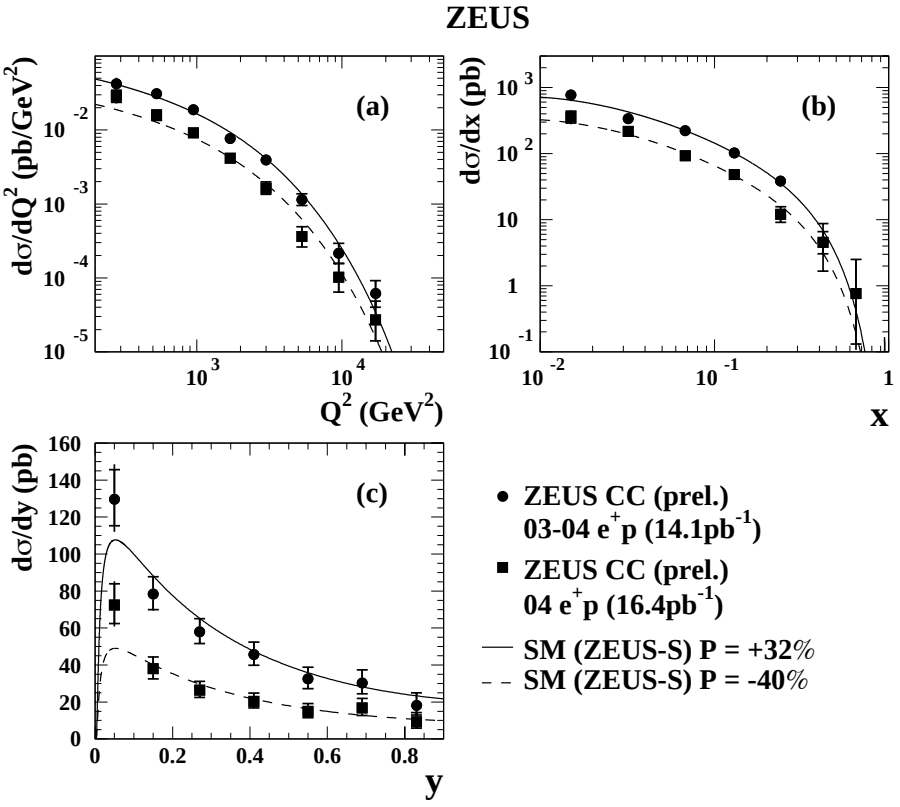

Figure 4: *The e^+p CC DIS cross-sections (a) $d\sigma/dQ^2$, (b) $d\sigma/dx$ and (c) $d\sigma/dy$. The circles (squares) represent data points for the positive (negative) polarisation measurements and the curves show the predictions of the SM evaluated using the ZEUS-S PDFs.*

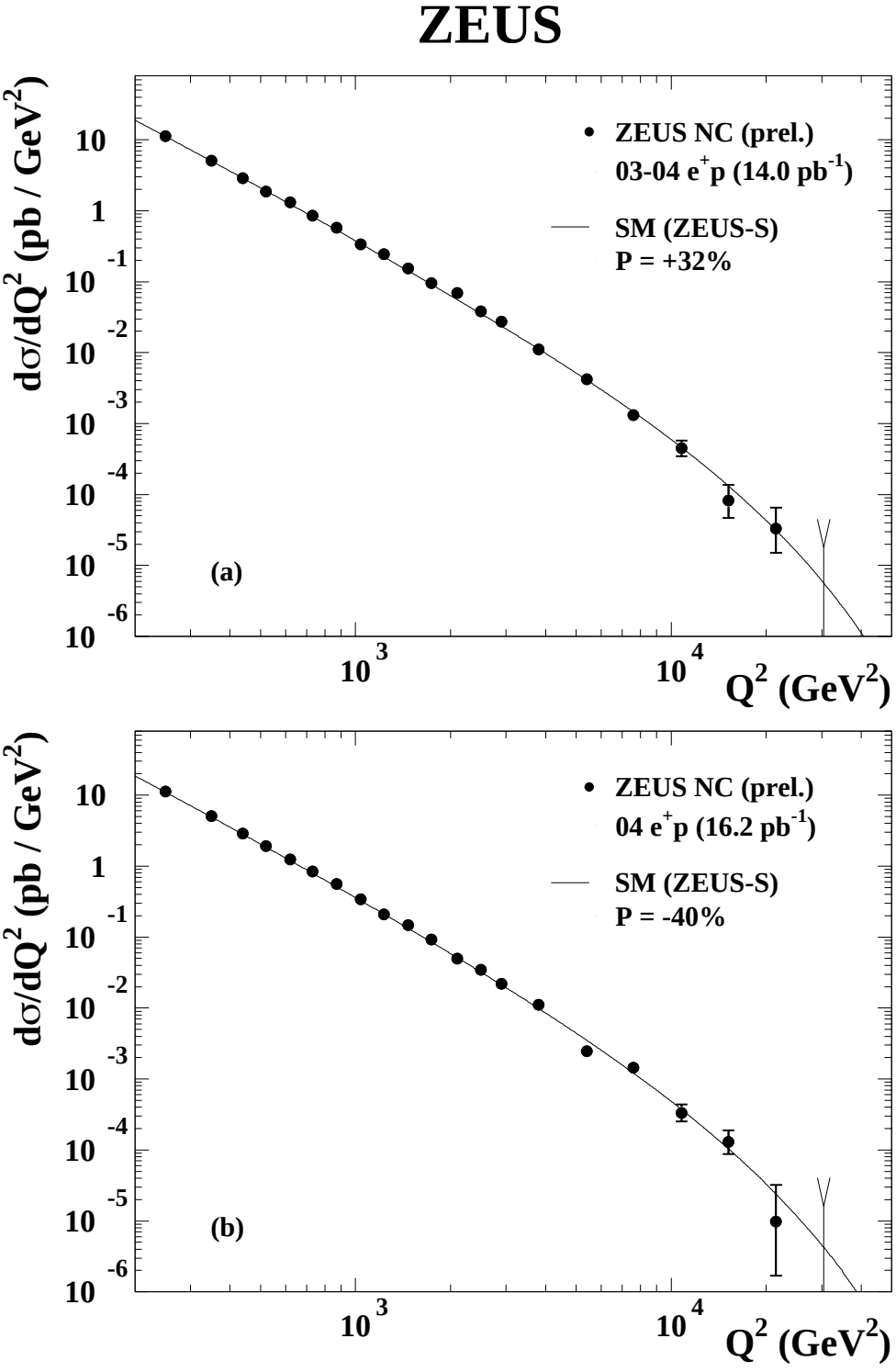

Figure 5: *The e^+p NC DIS cross-section $d\sigma/dQ^2$ for (a) positive polarisation data and (b) negative polarisation data. The lines show the predictions of the SM evaluated using the ZEUS-S PDFs.*

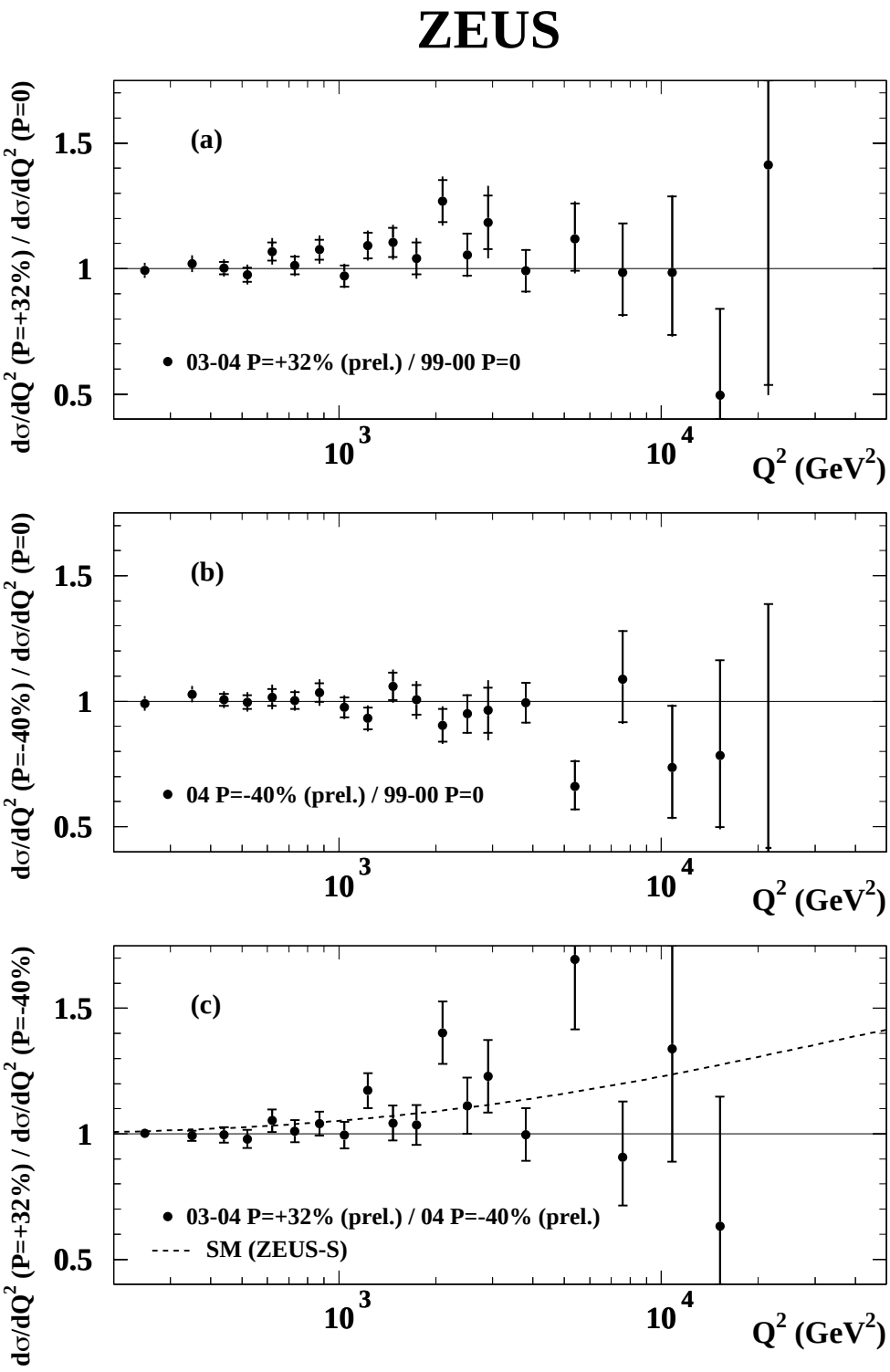

Figure 6: *Ratios of e^+p NC DIS cross-sections $d\sigma/dQ^2$ for (a) positively polarised data and unpolarised data, (b) negatively polarised data and unpolarised data and (c) positively and negatively polarised data. The dashed line shows the prediction of the SM evaluated using the ZEUS-S PDFs.*